Finite SNR Diversity-Multiplexing Trade-off in Hybrid ABCom/RCom-Assisted NOMA Networks

Xingwang Li, *Senior Member, IEEE,* Yike Zheng, *Student Member, IEEE,* Jianhua Zhang, *Senior Member, IEEE,* Shuping Dang, *Member, IEEE,* Arumugam Nallanathan, *Fellow, IEEE,* and Shahid Mumtaz, *Senior Member, IEEE*

***Abstract*—The upcoming sixth generation (6G) driven Internet-of-Things (IoT) will face the great challenges of extremely low power demand, high transmission reliability and massive connectivities. To meet these requirements, we propose a novel hybrid ambient backscatter communication (ABCom) or relay communication (RCom) *assisted non-orthogonal multiple access (NOMA) network*, which simultaneously enables traditional relay networks and ABCom-assisted IoT networks. Specifically, we investigate the reliability and the finite signal-to-noise ratio (SNR) diversity-multiplexing trade-off (f-DMT) of the proposed system to characterize the outage performance of the proposed system in the non-asymptotic SNR region. We derive the outage probability (OP) and the finite SNR diversity gain when two sources aim to communicate through either ABCom or RCom. On the basis that the results of Monte Carlo simulation and analysis are in perfect agreement, we discover that in the high SNR regime, the OP for ABCom tends to be a constant, leading to a zero diversity gain and an error floor, while the OP for RCom is monotone decreasing with respect to the SNR. Also, compared with the imperfect successive interference cancellation (ipSIC) mode, the reliability of the system under the ideal condition is significantly improved; Moreover, in the lower multiplexing gain regime, for both ABCom and RCom, the higher finite SNR diversity gain results in better system reliability, which provides good opportunities for ABCom to adapt f-DMT and improve relevant performance metrics by adapting the reflection parameter.**

***Index Terms*—Ambient backscatter communication, diversity-multiplexing trade-off, non-orthogonal multiple access, outage probability, two-way cooperative relaying.**

The work was supported in part by the National Natural Science Foundation of China under Grant 92167202, in part by the Open Foundation of State key Laboratory of Networking and Switching Technology (Beijing University of Posts and Telecommunications) under Grant SKLNST-2021-1-21, in part by the "Double First-Class" Discipline Creation Project of Surveying Science and Technology under Grant GCCRC202306, in part by Key Research and Development Project of Henan Province under Grant 231111210500.

X. Li and Y. Zheng are with the School of Physics and Electronic Information Engineering, Henan Polytechnic University and with the Jiaozuo Key Laboratory of Crow-Sensing Network, Jiaozuo, 454003, China. X. Li is also with the State Key Laboratory of Networking and Switching Technology, Beijing University of Posts and Telecommunications, Beijing 100876, China. (e-mail:lixingwangbupt@gmail.com, zhengyikehpu@163.com).

J. Zhang is with the State Key Laboratory of Networking and Switching Technology, Beijing University of Posts and Telecommunications, Beijing 100876, China (e-mail: jhzhang@bupt.edu.cn).

S. Dang is with the Department of Electrical and Electronic Engineering, University of Bristol, Bristol BS8 1UB, U.K. (e-mail: shuping.dang@bristol.ac.uk).

A. Nallanathan is with the School of Electronic Engineering and Computer Science, Queen Mary University of London, London E1 4NS, U.K. (email:a.nallanathan@qmul.ac.uk)

S. Mumtaz is with Department of Applied Informatics Silesian University of Technology Akademicka 1644-100 Gliwice, Poland and Nottingham Trent University Department of Engineering, Bristol, 4HTK, UK (dr.shahid.mumtaz@ieee.org).

I. Introduction

RECENTLY, the Internet of Things (IoT) has been booming around the world driven by the fifth generation (5G) mobile communications, and it is predicted that the number of IoT connected devices will increase from 21 billion in 2017 to 125 billion in 2030 [1]. To fulfill the device connectivity requirements, major countries around the world have focused on the studies of the sixth generation (6G) mobile communication technologies. Nevertheless, high energy consumption, as well as the shortage of spectrum resources, yields negative effects on intelligent connection of IoT devices. Therefore, energy-saving communications, also known as the extremely low-power communications or green communications, has proceeded for 6G networks [2]. As a consequence, various prospective technologies have been proposed to support extremely low-power communications with massive devices connected, for example, ambient backscatter communication (ABCom) [3], non-orthogonal multiple access (NOMA) [4], and cooperative relaying [5].

Because of the performance advantages in power consumption, spectral utilization, and deployment flexibility, ABCom reveals its significance as one of the solutions to the challenges apropos of extremely low-power communications [6]. Based on these characteristics, ABCom has become one of the research hotspots in academia in recent years [7–9]. The concept of ABCom was initially raised in [10] as a groundbreaking technology for diverse wireless application scenarios. In ABCom, backscatter device (BD) modulates and reflects its own signal to the reader with the aid of the surrounding radio frequency (RF) signals, such as TV, cellular and Wi-Fi signals [11]. In the meantime, the realization of such a self-sufficient ABCom system, which can operate in certain harsh scenarios without reliable power supplies for wireless transmissions, needs to work out the two main challenges of signal interference and security and reliability, which is also the motivation of this research.

More in-depth investigations of ABCom can be found in [12–15]. In [12], the authors put forward a frame system of cognitive ABCom coexisting with illegal eavesdroppers to explore the reliability and security of the proposed framework. Yang *et al.* in [13] proposed a cooperative ABCom system by considering two kinds of fading channels to explore the potential capacity for the low-power IoT. Considering the ABCom network with multiple BDs in [14], a backscattering link is randomly selected to reflect received signal so as

to minimize the outage probability (OP) of the backscattering link. In order to explore the reliability and security performance of practical NOMA-assisted cognitive ABCom networks, the authors in [15] considered the in-phase and quadrature-phase imbalance at RF front-ends and the existence of an eavesdropper. In addition, ABCom has been widely used in smart home, intelligent transportation systems and other fields [16, 17]. The authors of [16] designed the first battery-free video streaming camera to collect energy from two light sources, outdoor and indoor, and backscatter video up to 13 frames per second over a distance of 150 feet. In [17], Hansini et al. proposed a secure backscatter communication between two smart cars in vehicle-mounted AD-hoc networking to provide users with comfortable and easy driving environment.

It is inevitable that the quantity of connected devices in IoT will maintain ever-growing in the future, which puts forward extremely challenging needs, such as high spectral efficiency and massive connectivity [18]. Actuated by this setting, NOMA has appealed to wide attention from the industry and academia in recent years [19]. Unlike the traditionary orthogonal multi-access (OMA), NOMA permits all served users to share the same frequency/time/code domain resources through power multiplexing. This is achieved by sending a superimposed signal from the transmitter and recovering each individual signal through successive interference cancellation (SIC) at multiple receivers [20]. In particular, it is also worth noting that NOMA can allocate less power to users with superior channel conditions and more power to users with inferior channel conditions, so as to achieve user fairness and improve the holistic performance of the system [21].

To further enhance the overall system performance, the design and exploration of NOMA assisted ABCom systems can not only resolve the matter of spectrum scarcity in communications, but also continue to exert the virtues of ABCom systems with low cost and energy consumption [22–24]. The authors of [22] proposed an ABCom-NOMA network and derived the analytical expressions of the OP and the ergodic capacity to analyze the relationship between cellular and IoT networks. In [23], the system performance of ABCom-NOMA networks was discussed by deducing the analytical expressions of the effective capacity of NOMA users and BD. Taking overall consideration of the more practical error factors such as imperfect SIC (ipSIC), channel estimation errors, and residual hardware impairment, Li *et al.* in [24] introduced an ABCom-NOMA network interfered by artificial noise and studied its physical layer security (PLS).

Recently, on account of the rapid progress of network topology for wireless communications, the present mode of communications has translated to an incorporation of decentralized and concentrated communication rather than the conventional unitary centralized communication, and sundry cooperative communication technologies are increasingly and widely applied [25–28]. Specifically, the destination node creates a virtual multiple-input-multiple-output (MIMO) system by sharing other users' antennas without the need to configure multiple antennas to gain diversity [29]. Cooperative relay technology makes full use of the broadcast characteristics of wireless communication, not only reduces the power consumption and bandwidth of the terminal without increasing the complexity of the system, but also significantly improves the spectrum efficiency, throughput and capacity of the system [30, 31].

The advantage of relay channel is that it can realize reliable communication between the source node and the destination node with the help of relay [32]. The cooperative relay paradigm has promising applications and has recently received research attention [33–35]. In [33], the authors designed a downlink NOMA system with cooperative full-duplex (DF) relay, in which a near user acts as the relay for a far user, and explored the reliability of the considered system by deducing the OP and ergodic sum rate when the power distribution of BS and relay is fixed. The authors of [34] proposed a cooperative NOMA network in which the base station communicates with two users through an energy-harvesting relay, and analyzed the influence of different NOMA power distribution strategies of fixed power distribution and cognitive radio on simultaneous wireless information and power transfer (SWIPT) systems. Designed the NOMA assisted cognitive radio (CR) ABCom network, Le *et al.* in [35] assumed that the relay node can simultaneously collect/decode and backscatter the received source signal, and derived the OP and ergodic capacity of the receiving node.

Although it is well known that cooperative communications is a suppositional or distributed manifestation of MIMO paradigm [36], however, the great deal of studies on MIMO systems concentrated on acquiring the maximum diversity gain or multiplexing gain. In fact, the acquisition of both single maximum gains is one-sided, making it untoward to contrast the performance between diversity and multiplexing schemes. As a consequence, the authors in [37] proposed a disruptive idea that two genres of gains can actually be realized synchronously in a known channel, but there is a trade-off between them, namely the diversity-multiplexing trade-off (DMT), which is a more realistic view to deal with both gains. To characterize this aspect, Narasimhan in [38] introduced a more practical performance metric called the finite SNR DMT (f-DMT). The research on the performance of f-DMT makes up for the deficiency of the research on the combined performance of diversity gain and multiplexing gain.

The f-DMT has been extensively discussed in [39–41] from different perspectives. In [39], by deducing the analytic expressions of the lower bound on OP and the f-DMT, the authors discussed the analog network coding protocol performance of channelless coding for two-way relay systems. To solve the challenge of spectrum deficiency in aviation industry, Tan *et al.* in [40] proposed a hybrid-duplex aeronautical communication system, which is composed of one full duplex terrestrial station and two half-duplex aerial stations. Then, the analytical OP and f-DMT expressions are obtained for the SIC detectors. The authors of [41] analyzed the DMT of the dynamic Quantified Mapping forward strategy of the half-duplex single relay network, and obtained the optimal DMT of the proposed relay network.

A. Motivation and Contributions

Although ABCom, NOMA and cooperative communication have been well discussed in the above literature, the research on hybrid ABCom or relay communication (RCom)-assisted NOMA networks is still in its infancy. Motivated by this, we propose a hybrid ABCom/RCom-assisted NOMA networks system, which incorporates RCom enabling conventional transmission and ABCom enabling short distance IoT network. Benefiting from the characteristics of low-power reflection communications, f-DMT is adopted as the performance evaluation metric since ABCom devices always operate in the low-to-moderate SNR regions. Therefore, f-DMT is an effective way to characterize the outage performance of ABCom assisted IoT networks.

To the best of our knowledge, there is no work on studying the f-DMT performance of the hybrid ABCom or RCom-assisted NOMA networks systems, and only a few relevant research works can be found in [42–44]. Zhang *et al.* in [42] first proposed an intelligent reflection surface (IRS) assisted MIMO system based on large random matrix theory and then derived the analytical expressions of OP and f-DMT of the considered system. However, it is obvious that IRS and ABCom are backscattering technologies with different characteristics, the studies on IRS cannot are applicable to ABCom. In [43], the authors put forward an opportunistic source selection scheme for ABCom assisted cooperative relay communication systems and derived the analytical expressions of OP for the relaying and backscattering transmission. Yet, NOMA and f-DMT were not involved in this study. Li *et al.* in [44] investigated the affect of in-phase and quadrature phase imbalance (IQI) on the reliability and security of ABCom-NOMA systems by deriving the analytical expressions of OP and intercept probability (IP). However, f-DMT were not taken into consideration.

Based on a large amount of research works on ABCom, NOMA, and cooperative communication, in order to support the communications of both cellular and IoT networks, this paper analyzes f-DMT of hybrid ABCom or RCom-assisted NOMA networks systems to explore the advantage of ABCom on the performance of NOMA-assisted relay systems for current IoT communications of lower power, and we adopt the traditional RCom system as the benchmark. The main contributions of this paper are summarized as follows:

- We propose a hybrid ABCom/RCom-assisted NOMA system to satisfy the ever-increasing demands of low-power transmission, high spectrum utilization, multi-scenario applicability, and multi-user connectivity, which incorporates two modes: ABCom and RCom, to complete the information exchange through backscattering or relay forwarding. In the short-distance communication, the ABCom mode can be used to achieve low-power communication, and in the service of remote communication can be used RCom mode, and can be switched according to the different needs of communication coverage, so as to expand the application range of the communication system.
- The analytical expressions for the OP of the transmit signal from the source to the NOMA users are calculated based on the statistical characteristic of signal to interference plus noise ratio (SINR). Based on these expressions, we probe into the reliability performance of the proposed network. The results show that in the high SNR regime, the OP for ABCom tends to be constant, leading to the zero diversity gain and the error floor, while the OP for RCom is monotone decreasing with respect to the SNR.
- To characterize the OP slope in the non-asymptotic SNR regions, the analytical expressions of the finite SNR diversity gain and the f-DMT are derived,. The simulation results indicate that, for both ABCom and RCom, the higher finite SNR diversity gain results in better system reliability. In addition, simulation results also indicate that we can adapt the reflection parameter of ABCom to manage the f-DMT in an efficient manner.

B. Organization and Notations

The rest of the paper is planned as follows. Section II depicts the model of the hybrid ABCom/RCom NOMA-assisted TW system. Section III formulates and analyzes the OP and f-DMT of the considered system. Section IV verifies the accuracy of the analysis in the previous section through computer simulations and presents the numerical results. Section V concludes the paper.

The following notations are used to indicate the special symbols used in the rest part of this paper. $Pr\left(\cdot\right)$ represents the probability of the random event enclosed. $f_X\left(\cdot\right)$ is denoted as the probability density function (PDF) with respect to random variable X. $\mathcal{CN}\left(\mu,\sigma^2\right)$ refers to the complex Gaussian random distribution with mean μ and variance σ^2. $K_v\left(\cdot\right)$ stands for the modified Bessel function of the second kind with order v. The whittaker function is denoted as $W_{\lambda,\mu}\left(\cdot\right)$. $E\left(\cdot\right)$ signifies the expectation of the random variable enclosed.

II. System Model

A novel hybrid ABCom/RCom NOMA-assisted TW system model operating over Nakagami-m fading channels is considered as illustrated in Fig. 1. Specifically, the system involves a hybrid of two modes, where two source nodes A and B can exchange information through either the ABCom mode or the RCom mode. To streamline our discussion and focus the work the following assumptions are made: 1) A single antenna is equipped at all nodes; 2) All channels follow independent Nakagami-m distributions.

In this configuration, we assume that it is difficult to obtain perfect CSI due to some practical factors, so the channel estimation method is introduced. For the ABCom system, we assume that the cascaded channels can be approximated as a single channel to facilitate channel estimation calculations [45, 46]. Then, we denote as $\hat{h}_n = \hat{h}_i\hat{h}_p$. By employing linear minimum mean square error (LMMSE), the channel coefficient can be written as follows:

$$h_p = \hat{h}_p + e_p, \tag{1}$$

where $\hat{h}_p$ stands for the estimated channel coefficient, and $e_p \sim \mathcal{CN}\left(0,\delta_e^2\right)$ represents the estimated error of channel h_p.

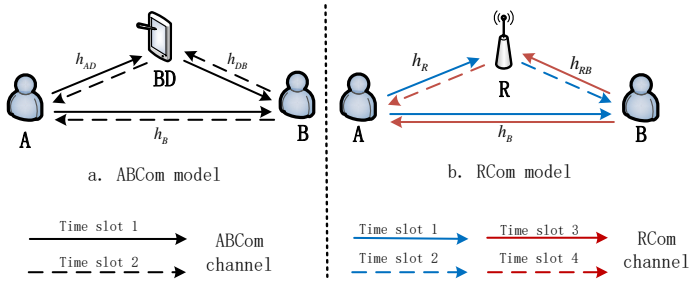

Fig. 1. System model of hybrid NOMA-assisted TW communications.

Further, $\hat{h}_p$ and e_p are independent and orthogonal because of the orthogonality of the LMMSE algorithm. The estimated channel power gains $\hat{h}_B$, $\hat{h}_R$, $\hat{h}_D$, and $\hat{h}_{RB}$ follow the gamma distributions with $E\left(\left|\hat{h}_B\right|^2\right) = \Omega_B$, $E\left(\left|\hat{h}_R\right|^2\right) = \Omega_R$, $E\left(\left|\hat{h}_{AD}\right|^2\right) = \Omega_{AD}$, $E\left(\left|\hat{h}_{DB}\right|^2\right) = \Omega_{DB}$, $E\left(\left|\hat{h}_{RB}\right|^2\right) = \Omega_{RB}$ and with fading parameters m_B, m_R, m_{AD}, m_{DB}, m_{RB}, respectively.

For ABCom, the entire information exchanging process is divided into two phases. In the first phase, node A communicates with node B through the direct and backscattering links. In the second phase, nodes A and B exchange identities. For RCom, the whole information exchange process is divided into four phases. In the first phase, node A transmits information through both of the direct link and the relaying link. In the second phase, node R sends information to node B using the DF relaying protocol. In a similar process, node B sends signals to node A in the third and fourth phases. Due to the symmetry of the system model and the reciprocity of the channel, the signal reception of node B is analyzed as an example without loss of generality. As detailed in [35], for the purpose of improving the quality of service for users and improving the spectrum efficiency, the NOMA technique is introduced. Then the transmitted signal of node B should be divided into two parts S_1 and S_2, whose power allocation coefficients are denoted as b and $1-b$, respectively, satisfying $b < 0.5$ and $E\left(|S_1|^2\right) = E\left(|S_2|^2\right) = 1$. The transmitted signal of node A can be expressed as

$$S_A = \sqrt{bP_A}S_1 + \sqrt{(1-b)P_A}S_2, \tag{2}$$

where P_A indicates the transmitted power of node A.

Then, the received signal at node B for ABCom can be expressed as [12]

$$y_B = \left(\hat{h}_B + e_B\right)S_A + \beta\left(\hat{h}_D + e_D\right)S_A c(t) + n_B, \tag{3}$$

where $c(t)$ represents the signal of BD, and β, which is used to normalize $c(t)$ with $E\left(|c(t)|^2\right) = 1$, is the reflection coefficient; n_B signifies the additive white Gaussian noise and $n_B \sim \mathcal{CN}\left(0, \sigma^2\right)$.

Similarly, the received signal at node i ($i \in (B, R)$) for RCom in the first time slot can be expressed as

$$y_i = \left(\hat{h}_i + e_i\right)S_A + n_i, \tag{4}$$

where n_i signifies the additive white Gaussian noise and $n_i \sim \mathcal{CN}\left(0, \sigma^2\right)$.

For RCom, considering the use of the DF relaying protocol at node R, the received signal in the second time slot of node B can be expressed as

$$y_{B_r} = \left(\hat{h}_{RB} + e_{RB}\right)S_R + n_{B_2}, \tag{5}$$

where $S_R = \sqrt{bP_r}S_1 + \sqrt{(1-b)P_r}S_2$, n_{B_2} signifies the additive white Gaussian noise and $n_{B_2} \sim \mathcal{CN}\left(0, \sigma^2\right)$, and P_r indicates the transmitted power of node R.

A. Received SINR

1) Received SINR for ABCom: Considering the NOMA process, node B first detects S_2 and treats S_1 and BD's signal as the interference. Thus, the received SINR at node B with respect to the detection of S_2 can be expressed as

$$\gamma_{S_2} = \frac{(1-b)\rho\left|\hat{h}_B\right|^2}{\rho b\left|\hat{h}_B\right|^2 + \delta_B^2\rho + \beta^2\rho\left|\hat{h}_D\right|^2 + \beta^2\rho\delta_D^2 + 1}, \tag{6}$$

where $\rho = \frac{P_A}{\sigma^2}$ stands for the transmitted SNR.

According to the protocol of NOMA, node B then decodes S_1 using SIC. In this study, we consider the practical conditions for the presence of ipSIC in the system [34]. Therefore, the instantaneous SINR at node B with respect to the detection of S_1 can be represented as

$$\gamma_{S_1} = \frac{b\rho\left|\hat{h}_B\right|^2}{(1-b)\rho\xi\left|\hat{h}_B\right|^2 + \delta_B^2\rho + \beta^2\rho\left|\hat{h}_D\right|^2 + \beta^2\rho\delta_D^2 + 1}, \tag{7}$$

where $\xi \in [0, 1]$ stands for the ipSIC parameter characterizing the severity of the imperfection. In particular, $\xi = 1$ and $\xi = 0$ represent no SIC and perfect SIC, respectively.

Similarly, when decoding signal $c(t)$ of BD, the instantaneous SINR can be written as

$$\gamma_c = \frac{\beta^2\rho\left|\hat{h}_D\right|^2}{\rho\xi|h_B|^2 + \delta_B^2\rho + \beta^2\rho\delta_D^2 + 1}, \tag{8}$$

2) Received SINR for RCom: In the first time slot, the received SINR at node i ($i \in \{B, R\}$) with respect to the detection of S_2 and S_1 can be expressed as

$$\gamma_{S_2}^i = \frac{(1-b)\rho\left|\hat{h}_i\right|^2}{b\rho\left|\hat{h}_i\right|^2 + \delta_i^2\rho + 1}, \tag{9}$$

and

$$\gamma_{S_1}^i = \frac{b\rho\left|\hat{h}_i\right|^2}{\xi(1-b)\rho\left|\hat{h}_i\right|^2 + \delta_i^2\rho + 1}, \tag{10}$$

respectively.

In the second time slot, the received SINR at node B with respect to the detection of S_2 and S_1 can be expressed as

$$\gamma_{S_2}^{B_2} = \frac{(1-b)\,\rho_r \left|\hat{h}_{RB}\right|^2}{b\rho_r |h_{RB}|^2 + \delta_{RB}^2 \rho_r + 1}, \tag{11}$$

and

$$\gamma_{S_1}^{B_2} = \frac{b\rho_r \left|\hat{h}_{RB}\right|^2}{\xi\,(1-b)\,\rho_r \left|\hat{h}_{RB}\right|^2 + \delta_{RB}^2 \rho_r + 1}, \tag{12}$$

respectively, where $\rho_r = \frac{P_r}{\sigma^2}$ stands for the transmitted SNR of node R, i.e., $\rho_r = \rho$.

III. Outage Performance and Finite-SNR DMT Analysis

In this section, we conduct a comprehensive analysis the reliability performance of the proposed hybrid ABCom/RCom NOMA-assisted TW system in terms of OP. Additionally, the asymptotic expression of OP in the high SNR region is also derived. Finally, we analyze and discuss the diversity gain d and multiplexing gain r for the proposed system, as well as the f-DMT to characterize outage performance at non-asymptotic SNRs. Both the finite SNR diversity gain and f-DMT measure the slope of OP at a given SNR. Specifically, given that wireless communication systems usually operate in low-to-moderate SNR regions, the expressions of the finite SNR diversity gain are derived enable a detailed analysis of the damping rate of OP and offer insights into the outage performance of the proposed hybrid systems.

A. Outage Performance Analysis for ABCom

The outage event can be defined as when the instantaneous rate of links is below the target rate.

1) Outage Probability of node B: Here, we study the complementary event of outage, which happens when the two following conditions are both satisfied: 1) S_2 can be successfully decoded by node B; 2) S_1 can be successfully decoded by node B. Therefore, the OP of node B for ABCom at a given target rate is defined by

$$P_{out}^{B} = 1 - Pr\left\{\log_2(1+\gamma_{S_2}) \geq R_1, \log_2(1+\gamma_{S_1}) \geq R_2\right\}. \tag{13}$$

In practice, two target rates R_1 and R_2 are generally different because of different quality-of-service (QoS) requirements. For the purposes of mathematical simplicity and comparison, we let $R_1 = R_2 = R$, and the same assumption can be found in [43].

Accordingly, multiplexing gain r determines how the given target rate R scales following the finite SNR and is given by [37]

$$r = \frac{R}{\log_2(1+\rho)}. \tag{14}$$

Next, we have the following theorem and an associated corollary to derive closed-form expression of the OP at node B.

Theorem 1. *For Nakagami-m fading channels, the analytical expression of OP of node B can be computed as*

$$P_{out}^{B}(\rho, r) = 1 - \sum_{n=0}^{m_B-1}\sum_{k=0}^{n} \frac{\bar{A}_1 A_e^k \bar{A}_2 \Delta_1^{k-\varpi_1} W_{\lambda,\upsilon}(\varpi_2)}{\beta^{2\varpi_1}\rho^k e^{-\frac{\varpi_2}{2}+\frac{A_e\Delta_1}{\rho\Omega_B}}}, \tag{15}$$

where $\theta = 2^R - 1 = (1+\rho)^r - 1$, $\Delta_1 = \max(\frac{\theta}{(1-b-\theta b)}, \frac{\theta}{[b-\theta\xi(1-b)]})$, $\varpi_1 = \frac{m_{AD}+m_{DB}-1}{2}$, $\lambda = -(n+\varpi_1-k)$, $\upsilon = \frac{m_{AD}-m_{DB}}{2}$, $\bar{A}_1 = \frac{C_n^k}{\Gamma(m_{AD})\Gamma(m_{DB})(\Omega_{AD}\Omega_{DB})^{\varpi_1} n!}$, $\bar{A}_2 = \frac{\Gamma(n+m_{AD}-k)\Gamma(n+m_{DB}-k)}{(\Omega_B)^{k-\varpi_1}}$, $\boldsymbol{A_e = \delta_B^2\rho + \delta_D^2\rho\beta^2 + 1}$, *and* $\varpi_2 = \frac{\Omega_B}{\Omega_{AD}\Omega_{DB}\Delta_1\beta^2}$.

Proof: See Appendix A. ∎

To gain deeper insights and conduct diversity gain analysis, we analyze the asymptotic expression of OP for node B in the high SNR regions.

Corollary 1. *Under the condition of high SNR, the asymptotic expression of OP of B can be written as*

$$P_{out,\rho\to\infty}^{B}(\rho, r) = 1 - \sum_{n=0}^{m_B-1}\sum_{k=0}^{n} \frac{\bar{A}_1 \bar{A}_2 \Delta_1^{k-\varpi_1} W_{\lambda,\upsilon}(\varpi_2)}{\beta^{2\varpi_1}\rho^k e^{-\frac{\varpi_2}{2}}}. \tag{16}$$

2) Outage Probability of BD: Similarly, BD can successfully decode the information when all the three following conditions are satisfied: 1) S_2 can be successfully decoded by node B; 2) S_1 can be successfully decoded by node B; 3) $c(t)$ can be successfully decoded by the BD. The OP of BD for ABCom at a given data rate R is thus defined in (16), which is given at the top of the next page.

Again, we have the following theorem and an associated corollary to derive closed-form expressions for the outage performance analysis of the BD.

Theorem 2. *For Nakagami-m fading channels, the analytical expression of the OP of BD can be calculated as*

$$P_{out}^{BD}(\rho, r) = P_{out}^{B}(\rho, r) + A_1 + A_2 - A_3, \tag{18}$$

where $\Delta_2 = A_e \max\left(\frac{\theta\varpi_5}{\beta^2\rho}, \frac{\theta}{\beta^2\rho}\right)$, $\bar{A}_3 = \frac{C_n^k \bar{A}_1 (\beta^2\rho)^{n-k} A_e^k}{N(\Omega_{AD}\Omega_{DB})^{\frac{1}{2}}\Omega_B{}^n}$, $\varpi_3 = \frac{m_{AD}+m_{DB}}{2} + n - k - 1$, $\varpi_4 = \frac{\Omega_B\theta\xi}{\beta^2\Omega_{AD}\Omega_{DB}}$, $\varpi_5 = \frac{\Delta_1\xi\rho+1}{1-\Delta_1\theta\xi\rho}$, $\varphi_i = \frac{\cos[(2i-1)\pi]}{2N}$, $\varphi_j = \frac{\cos[(2j-1)\pi]}{2K}$, $B_1 = \frac{\Delta_2(\varphi_i+1)}{2}$, $A_1 = \sum_{n=0}^{m_B-1}\sum_{k=0}^{n}\sum_{i=0}^{N} \frac{\pi\Delta_1^n \bar{A}_3 \Delta_2 \sqrt{1-\varphi_i{}^2}}{B_1^{-\varpi_3} e^{\frac{B_1\Delta_1\beta^2+A_e\Delta_1}{\rho\Omega_B}}} K_{2\upsilon}\left(2\sqrt{B_3}\right)$, $A_2 = \sum_{n=0}^{m_B-1}\sum_{k=0}^{n} \frac{(-1)^k \bar{A}_1 \bar{A}_2 A_e^k \beta^{2\varpi_1}\theta^{\varpi_1}}{\xi^{k-\varpi_1}\rho^k e^{\frac{\varpi_4}{2}-\frac{A_e}{\Omega_B\xi\rho}}} W_{\lambda,\upsilon}(\varpi_4)$, $B_2 = \frac{\Delta_2(\varphi_j+1)}{2}$, $B_3 = \frac{B_1}{\Omega_{AD}\Omega_{DB}}$, $A_3 = \sum_{n=0}^{m_B-1}\sum_{k=0}^{n}\sum_{j=0}^{K} \frac{\pi(-1)^k \bar{A}_3 \Delta_2 B_2^{\varpi_3}\sqrt{1-\varphi_j{}^2}}{(\theta A_e)^{n-k}(\xi\rho)^n e^{\frac{B_2\beta^2\rho+\theta A_e}{\Omega_B\theta A_e\xi\rho}}} K_{2\upsilon}\left(2\sqrt{B_4}\right)$, $B_4 = \frac{B_2}{\Omega_{AD}\Omega_{DB}}$, *and N and K are the accuracy-complexity trade-off parameters.*

Proof: See Appendix B. ∎

To obtain more insights and as well as to carry out the diversity gain analysis, we analyze the asymptotic expression of OP of node BD in the high SNR region.

$$P_{out}^{BD} = 1 - Pr\left\{\log_2\left(1+\gamma_{S_2}\right) \geq R, \log_2\left(1+\gamma_{S_1}\right) \geq R, \log_2\left(1+\gamma_c\right) \geq R\right\} \tag{17}$$

Corollary 2. *Under the condition of high SNR, we can obtain the asymptotic expression of OP for BD as*

$$P_{out,\rho\to\infty}^{BD}(\rho,r) = P_{out,\rho\to\infty}^{B}(\rho,r) + A_1^{\infty} + A_2^{\infty} - A_3^{\infty}, \tag{19}$$

where $A_1^{\infty} = \sum_{n=0}^{m_B-1}\sum_{k=0}^{n}\sum_{i=0}^{N}\frac{(-1)^{2\upsilon}\pi A_e\bar{A}_3\Delta_2{\Delta_1}^n\sqrt{1-{\varphi_i}^2}}{\Gamma(2\upsilon+1){B_1}^{-\varpi_3}{B_3}^{-\upsilon}\left(1-\ln\sqrt{B_3}\right)^{-1}}$,
$A_2^{\infty} = \sum_{n=0}^{m_B-1}\sum_{k=0}^{n}\frac{(-1)^k\bar{A}_1\bar{A}_2A_e\beta^{2\varpi_1}}{\theta^{-\varpi_1}\rho^k\xi^{k-\varpi_1}e^{\frac{\varpi_4}{2}}}W_{\lambda,\upsilon}(\varpi_4)$, *and*
$A_3^{\infty} = \sum_{n=0}^{m_B-1}\sum_{k=0}^{n}\sum_{j=0}^{K}\frac{(-1)^k\pi\bar{A}_3A_e\Delta_2\sqrt{1-{\varphi_j}^2}}{\theta^{n-k}\xi^n\rho^k{B_2}^{-\varpi_3}{B_4}^{-\upsilon}}\ln\left(\sqrt{B_4}\right)$.

Proof: When $x \to 0$, employing the approximate expression of the exponential function $e^x \approx 1+x$ and the zero-order Bessel function of the second kind $K_0(x) \approx -\ln\left(\frac{x}{2}\right)$ and performing a series of basic mathematical manipulations, we can approximate $e^{-\frac{B_1\Delta_1\beta^2+A_e\Delta_1}{\Omega_B\rho}} \overset{\rho\to\infty}{\approx} 1$, and $K_{2\upsilon}\left(2\sqrt{B_3}\right) \overset{\rho\to\infty}{\approx} \frac{(-1)^{2\upsilon}B_3^{\upsilon}}{\Gamma(2\upsilon+1)}\left(1-\ln\sqrt{B_3}\right)$, and $e^{-\frac{\varpi_4}{2}+\frac{A_e}{\Omega_B\xi\rho}} \overset{\rho\to\infty}{\approx} e^{-\frac{\varpi_4}{2}}$, by which we can obtain (18). ■

Remark 1. *From **Theorem 1**, **Theorem 2**, **Corollary 1** and **Corollary 2**, it becomes evident that with the increase of SNR, the OP gradually decreases until it tends to a non-zero constant. This implies the existence of an outage floor of the proposed system with the presence of ipSIC and ipCSI. Therefore, the quality of SIC and CSI is of paramount importance for the reliability of the proposed NOMA-assisted TW-ABCom system.*

B. Outage Performance Analysis for RCom

Based on the NOMA and DF relaying protocol, it can be known that for node B or node R, when the decoding signal of either S_1 or S_2 fails, the outage event will occur at node B, the OP at node B for RCom can thus be expressed as

$$P_{out}^{BR} = \left(1-P_o^{BR_1}\right)\left(1-P_o^{BR_2}\right), \tag{20}$$

where $P_o^{BR_1}$ and $P_o^{BR_2}$ represent the probability of node B successfully decoding signals S_1 and S_2 in the first and second time slots, respectively.

Next, we have the following theorem to derive the closed-form expression of the OP at node B for RCom.

Theorem 3. *For Nakagami-m fading channels, the analytical expression for the OP of node B for RCom can be computed as*

$$P_{out}^{BR}(\rho,r) = \left(1-\frac{\Gamma\left(m_B,\frac{\Delta_R m_B}{\Omega_B\rho}\right)}{\Gamma(m_B)}\right) \times \left(1-\frac{\Gamma\left(m_R,\frac{\Delta_R m_R}{\Omega_R\rho}\right)\Gamma\left(m_{RB},\frac{\Delta_R m_{RB}}{\Omega_{RB}\rho}\right)}{\Gamma(m_R)\Gamma(m_{RB})}\right), \tag{21}$$

where $\Delta_R = \max\left(\frac{\theta\left(\delta_B^2\rho+1\right)}{1-b-b\theta}, \frac{\theta\left(\delta_B^2\rho+1\right)}{b-(1-b)\theta}\right)$.

Proof: See Appendix C. ■

Remark 2. *From **Theorem 3**, we can discover that, it becomes evident that the OP decreases, the reliability performance of the system is thereby improved. Different from the outage performance as analyzed for the BD, there does not exist an outage floor at node B, and, hence, a non-zero diversity order is achievable.*

C. Finite SNR DMT Analysis for ABCom

The finite SNR diversity gain has been regarded as an important criterion to evaluate the outage probability slope at particular SNR levels, which is defined as the negative slope of the log-log plot of OP with respect to SNR [38]. Then, the mathematical definitions and derivation processes related to the f-DMT at variable data rate are provided. The DMT is the essential trade-off of any communication systems, reflecting the key relation between transmission efficiency and reliability characterized by multiplexing gain r and diversity gain d, respectively.

The diversity order, also known as the diversity gain under infinite SNR, can be used to characterize the effect of system and fading parameters on the OP of the proposed NOMA network, and thus to further estimate the reliable performance of the system, which can be understood as the rate at the high SNR regions the OP decays with the increase of SNR.

According to [24], we have the following definition of the diversity order as

$$d = -\lim_{\gamma\to\infty}\frac{\log P_{out,\gamma\to\infty}}{\log\gamma}. \tag{22}$$

Corollary 3. *The diversity orders of node B and the BD for ABCom can be obtained according to (15), (21), and (27) as*

$$d_B = d_{BD} = 0. \tag{23}$$

Meanwhile, according to [38], the finite SNR diversity gain can be expressed as

$$d(\rho,r) = -\frac{\rho}{P_{out}(\rho,r)}\frac{\partial P_{out}(\rho,r)}{\partial\rho}. \tag{24}$$

Simultaneously, for the sake of mathematical realizability, we assume that the CSI is known in the following DMT derivation.

Theorem 4. *The analytical expression for the finite SNR diversity gain of node B for ABCom can be computed as follows:*

- *When* $\Delta_1 = \frac{\theta}{C_1}$, *we have*

$$d_B(\rho,r) = -\frac{\rho}{P_{out}^{B}(\rho,r)}U_1, \tag{25}$$

where

$$U_1 = -\sum_{n=0}^{m_B-1}\sum_{k=0}^{n}\varepsilon_1\frac{\left(D_2 W_{\lambda,\upsilon}\left(\varpi_2\right)-D_3\right)}{\rho e^{\frac{\Delta_1}{\rho\Omega_B}-\frac{\varpi_2}{2}}}, \quad (26)$$

$\varepsilon_1 = \frac{\bar{A}_1\bar{A}_3\Delta_2}{\beta^2\varpi_1}$, $B_5 = W_{\lambda,\upsilon}\left(\varpi_2\right)\left(\lambda-\frac{\varpi_2}{2}\right) - \left[\upsilon^2-\left(\lambda-\frac{1}{2}\right)^2\right]W_{\lambda-1,\upsilon}\left(\varpi_2\right)$, $B_6 = k-\varpi_1-1$, $D_1 = \frac{1-\theta\left[(\rho C_2)^{-1}-bC_1^{-1}\right]}{\Omega_B\rho C_1 C_2^{-1}} + \frac{\varpi_2 C_2(1-b)}{2\theta C_1}$, $D_2 = \frac{(B_6-1)(1-b)C_2-\left(k\rho^{-1}+D_1\right)C_1\theta^{-1}}{\rho^k C_1^{2B_6}\theta^{-B_6}}$, $D_3 = \frac{B_5(1-b)C_2}{C_1^{B_6+1}\theta^{-B_6}\rho^k}$, $C_1 = 1-b(1+\rho)^r$, *and* $C_2 = r(1+\rho)^{r-1}$.

- *When* $\Delta_1 = \frac{\theta}{C_3}$, *we can similarly derive*

$$d_B\left(\rho,r\right) = -\frac{\rho}{P_{out}^B\left(\rho,r\right)}U_1, \quad (27)$$

where

$$U_1 = -\sum_{n=0}^{m_B-1}\sum_{k=0}^{n}\frac{\varepsilon_1\left(D_5 W_{\lambda,\upsilon}\left(\varpi_2\right)-D_6\right)}{\rho e^{\frac{\Delta_1}{\rho\Omega_B}-\frac{\varpi_2}{2}}}, \quad (28)$$

$C_3 = b-\xi\left(1-b\right)\theta$, $D_4 = \frac{b\rho C_2-\theta C_3}{\Omega_B(\rho C_3)^2} + \frac{b\varpi_2 C_2}{2\theta C_3}$, $D_5 = \frac{(B_6-1)bC_2-\left(k\rho^{-1}-D_4\right)C_3\theta}{C_3{}^{B_6+2}\rho^{k-1}\theta^{-B_6}}$, *and* $D_6 = \frac{bC_2B_5\theta^{B_6}}{C_3^{-B_6+2}\rho^k}$.

Proof: The proof of **Theorem 4** can be completed by simply taking the derivative of (14) with respect to ρ. ■

Similarly, we have the following theorem to derive the analytical expression of the finite SNR diversity gain of node BD for ABCom.

Theorem 5. *The analytical expression for the finite SNR diversity gain of BD for ABCom can be computed as*

$$d_{BD}\left(\rho,r\right) = \frac{\rho}{P_{out}^{BD}\left(\rho,r\right)}\left(U_1+I_1+I_2-I_3\right), \quad (29)$$

where

$$I_1 = \sum_{n=0}^{m_B-1}\sum_{k=0}^{n}\frac{(-1)^k\varepsilon_2\theta^{\varpi_1}e^{\frac{\varpi_4}{2}+\frac{1}{\Omega_B\xi\rho}}}{\rho^k\left(W_{\lambda,\upsilon}\left(\varpi_4\right)Q_7+\frac{C_2Q_8}{\theta}\right)^{-1}}, \quad (30)$$

- *When* $\Delta_1 = \frac{\theta}{\rho C_1}$ *and* $\Delta_2 = \frac{\theta\varpi_5}{\beta^2\rho}$, *the expressions of* I_2 *and* I_3 *can be calculated by*

$$I_2 = \sum_{n=0}^{m_B-1}\sum_{k=0}^{n}\sum_{i=0}^{N}V_1D_7\left(Q_1-E_1-\frac{\theta^nB_{10}Q_4Q_{17}}{\rho^k\Omega_B{C_1}^{n-1}}\right), \quad (31)$$

$$I_3 = \sum_{n=0}^{m_B-1}\sum_{k=0}^{n}\sum_{j=0}^{K}V_2\theta^{k-n}\left(Q_{12}-E_2-\frac{Q_9Q_{15}}{\rho^k\sqrt{B_4}}\right), \quad (32)$$

where $B_7 = B_1^{\varpi_3}e^{-\frac{\theta\left(B_1\beta^2\rho+1\right)}{\rho C_1\Omega_B}}$, $B_8 = 2\xi\theta+C_1-b\theta$, $B_9 = \xi\theta+C_1$, $B_{10} = \varphi_i+1$, $B_{11} = \varphi_j+1$, $\varepsilon_2 = \frac{\bar{A}_3N\pi}{\xi^n\rho^{n-k}}$, $V_1 = \frac{\varepsilon_2\sqrt{1-{\varphi_i}^2}}{N}$, $V_3 = \frac{\varepsilon_2\sqrt{1-\varphi_j^2}}{K}$, $D_7 = K_{2\upsilon}\left(\sqrt{4B_3}\right)B_8$, $D_8 = \frac{(k+1)D_{10}-\rho^kC_2\left(Q_{14}+nbC_1^{-1}D_{10}\right)}{\rho^{-k}{C_1}^{-n}}$, $D_9 = D_{11}C_1-\rho bC_2D_{10}$, $D_{10} = C_1-\theta^2\xi$, $D_{11} = D_{10}-\rho C_2Q_{14}$, $Q_1 = \frac{C_2\rho^{k+1}(B_8+nB_9)D_{10}-\theta B_9D_8}{\beta^2{C_1}^n\rho^{k+n+2}D_{10}^2\theta^{-n}}$, $Q_2 = \frac{B_{10}\varpi_5\left[(B_8+B_9)\theta\rho C_2C_1D_{10}-B_9\theta^2D_9\right]}{2\Omega_B\rho^2D_{10}^2{C_1}^2}$, $Q_3 = \frac{C_2\rho C_1-\theta(C_1-\rho bC_2)}{\Omega_B(\rho C_1)^2}$, $Q_4 = \frac{C_2\rho B_8D_{10}-B_9\theta D_{11}}{2\beta^2\rho^2D_{10}^2}$, $Q_5 = \frac{\Omega_B\xi k\rho+1}{\Omega_B\xi\rho^2}$, $Q_6 = K_{2\upsilon-1}\left(2\sqrt{B_3}\right)+K_{2\upsilon+1}\left(2\sqrt{B_3}\right)$, $Q_7 = \frac{(2\varpi_1+\varpi_4)C_2}{2\theta}-Q_5$, $Q_8 = \left(\lambda-\frac{\varpi_4}{2}\right)W_{\lambda,\upsilon}\left(\varpi_4\right) - \left[\upsilon^2-\left(\lambda-\frac{1}{2}\right)^2\right]W_{\lambda-1,\upsilon}\left(\varpi_4\right)$, $Q_9 = \frac{K_{2\upsilon}\left(2\sqrt{B_4}\right)}{B_2^{-\varpi_3}e^{\frac{\theta B_2\beta^2\rho-\theta}{\Omega_B\rho\xi}}}$, $Q_{10} = D_{11}+kD_{10}$, $Q_{11} = \left[B_9\left(k-n\right)+B_8\right]\theta^{k-n}C_2$, $Q_{12} = \frac{\left(Q_{11}\rho D_{10}-\theta^{1+k-n}B_9Q_{10}\right)Q_9}{\beta^2\rho^{k+2}D_{10}^2}$, $Q_{13} = \frac{B_{11}[(\xi-b)\rho C_2D_{10}-B_9D_{11}]+2D_{10}^2}{2\Omega_B\xi(\rho D_{10})^2}$, $Q_{14} = b+2\theta\xi$, $Q_{15} = K_{2\upsilon-1}\left(2\sqrt{B_4}\right)+K_{2\upsilon+1}\left(2\sqrt{B_4}\right)$, $Q_{16} = \frac{B_{11}Q_4}{2\rho\Omega_B\xi}K_{2\upsilon}\left(2\sqrt{B_4}\right)$, $Q_{17} = \frac{B_7Q_5Q_6B_{10}}{2\sqrt{B_3}D_7}$, $E_1 = \frac{Q_2+Q_3\varpi_5+\varpi_3Q_4B_{10}B_1^{-1}}{\rho^{k+1}\theta^{-n-1}\beta^2{C_1}^n}$, *and* $E_2 = \frac{Q_9\theta\varpi_5Q_{13}+2\rho\varpi_3Q_4Q_9\beta^2}{\rho^{k+1}\beta^2}$.

- *When* $\Delta_1 = \frac{\theta}{\rho C_1}$ *and* $\Delta_2 = \frac{\theta}{\beta^2\rho}$, I_2 *and* I_3 *can be rewritten as*

$$I_2 = \sum_{n=0}^{m_B-1}\sum_{k=0}^{n}\sum_{i=0}^{N}V_1D_7\left(C_5+\frac{\theta^{n+1}E_3}{C_1^n\rho^{k+1}\beta^2}\right), \quad (33)$$

$$I_3 = \sum_{n=0}^{m_B-1}\sum_{k=0}^{n}\sum_{j=0}^{K}V_3Q_9\left(C_7+E_4-E_5\right), \quad (34)$$

where $C_5 = \frac{(1+n)\theta^{-1}-(1+k)(C_2\rho)^{-1}+nbC_1^{-1}}{(C_2\theta^{n+1})^{-1}\beta^2\rho^{k+1}{C_1}^{2-n}}$, $C_6 = Q_3\left(B_{10}\theta+1\right) + \frac{\theta(C_1-\rho bC_2)}{2\Omega_B(C_1\rho)^2}$, $C_7 = \frac{(1+k-n)C_2\rho-(1+k)\theta}{\beta^2\rho^{k+2}\theta^{n-k}}$, $E_3 = \frac{\varpi_3(C_2\rho-\theta)-\theta C_6}{\theta}+Q_{17}\varsigma_3$, $E_4 = \frac{\beta^2B_2\theta^{k-n}+\Omega_B\xi\varpi_3(C_2\rho-\theta)}{\Omega_B\xi\beta^2\rho^{k+2}}$, $E_5 = \frac{\theta^{k-n}Q_{15}\varsigma_3B_2{}^{\varpi_3+\frac{1}{2}}}{Q_9\rho^ke^{\frac{B_2\rho\beta^2-\theta}{\Omega_B\theta\xi\rho}}}$.

- *When* $\Delta_1 = \frac{\theta}{\rho C_3}$ *and* $\Delta_2 = \frac{\theta}{\beta^2\rho}$, *the expressions of* I_2 *and* I_3 *can be calculated as*

$$I_2 = \sum_{n=0}^{m_B-1}\sum_{k=0}^{n}\sum_{i=0}^{N}V_1D_7\left(C_5{C_1}^{2-2n}-\frac{\theta^{n+1}E_6}{C_3^n\beta^2\rho^{n+1}}\right), \quad (35)$$

$$I_3 = \sum_{n=0}^{m_B-1}\sum_{k=0}^{n}\sum_{j=0}^{K}V_3Q_9\left(\varsigma_4+E_4-E_7\right), \quad (36)$$

where $\varsigma_1 = B_{10}\theta^2\left[b\rho C_2-\theta C_1\right]+3C_1\theta$, $\varsigma_2 = \frac{\varsigma_1}{2\Omega_B(C_1\rho)^2}+2Q_3$, $\varsigma_3 = \frac{C_2\rho-\theta}{2\beta^2\Omega_{AD}\Omega_{DB}\rho^2}$, $\varsigma_4 = \frac{(1+k-n)C_2\rho-(1+k)\theta}{\beta^2\rho^{k+2}\theta^{n-k}}$, $E_6 = \varsigma_2+\frac{\varpi_3(\rho A_2-\theta)}{\rho\theta}-\varsigma_3Q_{17}$, *and* $E_7 = \frac{Q_{15}\varsigma_3B_4{}^{\varpi_3+\frac{1}{2}}}{Q_9\theta^{n-k}\rho^ke^{\frac{B_4\rho\beta^2-\theta}{\Omega_B\theta\xi\rho}}}$.

- *When* $\Delta_1 = \frac{\theta}{\rho C_3}$ *and* $\Delta_2 = \frac{\theta\varpi_5}{\beta^2\rho}$, *the following expressions* I_2 *and* I_3 *can be derived as*

$$I_2 = \sum_{n=0}^{m_B-1}\sum_{k=0}^{n}\sum_{i=0}^{N}V_1D_7\left(\varsigma_7-E_8+\frac{\theta^n\varpi_3\varsigma_{11}}{C_3^n\rho^n}\right), \quad (37)$$

$$I_3 = \sum_{n=0}^{m_B-1}\sum_{k=0}^{n}\sum_{j=0}^{K}\frac{V_3Q_9}{\rho^k\theta^{n-k}}\left(\frac{\varsigma_{17}\rho^k}{\theta^{k-n}}-E_9-\frac{Q_{15}\varsigma_{18}}{Q_9\sqrt{B_4}}\right), \quad (38)$$

where $B_{12} = 2\theta+\left(1+n-\theta^2\xi{C_3}^{-1}\right)(1-b)$, $\varepsilon_3 = C_3-\theta^2\xi$, $\varepsilon_4 = \theta\xi+C_3$, $\varsigma_5 = (k+1)\rho^{-1}-C_2\xi\varepsilon_3{}^{-1}B_{12}$, $\varsigma_6 = \xi\theta b+\varepsilon_4\left(1+n\right)$, $\varsigma_7 = \frac{C_2\varsigma_6-\theta\varepsilon_4\varsigma_5}{\rho^{k+1}\beta^2{C_3}^n\varepsilon_3\theta^{-n}}$, $\varsigma_8 =$

$C_3\left(C_4+\varsigma_{10}-\theta^2\xi C_4\right)$, $C_4 = -(1-b)\rho\xi C_2$, $\varsigma_9 = \frac{[(2+b)\xi\theta+2C_3\rho C_2]\theta C_3\varepsilon_3-\theta^2\varepsilon_4\varsigma_{14}}{\Delta_2\Omega_B B_1^{-1}(\rho C_3\varepsilon_3)^2}$, $\varsigma_{10} = \varepsilon_3 + C_4 - 2\theta C_2\xi\rho$, $\varsigma_{11} = \frac{C_2\rho b(1+2\xi\theta)\varepsilon_3-\varepsilon_4\theta\varsigma_{10}}{\beta^2\rho^{n-k+2}\varepsilon_3^2}$, $\varsigma_{13} = \frac{\rho C_2C_3-\theta(C_3+\theta)}{\Omega_B(\rho C_3)^2}$, $\varsigma_{12} = \frac{C_2b\varepsilon_3-\varepsilon_4\theta\varsigma_{10}}{\Delta_2\beta^2(\varepsilon_3\rho)^2}$, $\varsigma_{14} = C_3\varepsilon_3 - 2\rho C_2C_3(1-b+n) + C_4\theta^2$, $\varsigma_{15} = (k+1)\varepsilon_3 + C_4 - 2\theta\xi C_2\rho$, $\varsigma_{16} = \frac{\varsigma_{14}\rho\varepsilon_3-\theta^{1+k-n}\varepsilon_4\varsigma_{15}}{\beta^2\rho^{k+2}\varepsilon_3^2}$, $\varsigma_{17} = \frac{[\varsigma_6+(k-2n)\varepsilon_4]C_2\rho-\theta\varepsilon_4\varepsilon_3^{-1}\varsigma_{15}}{\beta^2\rho^{k+2}\varepsilon_3\theta^{n-k}}$, $\varsigma_{18} = \frac{bC_2\rho\varepsilon_3-\varepsilon_4\varsigma_{10}}{\beta^2(\rho\varepsilon_3)^2}$, $\varsigma_{19} = \frac{\rho C_2C_3-\theta(C_3+C_4)}{\Omega_B\rho^2{C_3}^2}$, $E_8 = \frac{\varpi_5(\varsigma_9+\varsigma_{19}+2Q_{17}\varsigma_{11})}{C_3^n\beta^2\theta^{-n-1}\rho^{2n-k+1}}$, *and* $E_9 = \frac{\theta\varpi_5\left(\Omega_B\rho^2\xi\varsigma_{18}-1\right)}{\beta^2\Omega_B\xi\rho^3} + \varpi_3\varsigma_{18}$.

Proof: The proof of **Theorem 5** can be completed by simply taking the derivative of (17) with respect to ρ. ■

Remark 3. *From **Corollary 3**, **Theorem 4** and **Theorem 5**, we can find that with the increase of SNR, the finite SNR diversity gain decreases, which is roughly consistent with the varying trend of the OP slope. In addition, from the perspective of f-DMT, a smaller multiplexing gain results in a higher finite SNR diversity gain.*

D. Finite-SNR DMT Analysis for RCom

For RCom, according to the definition in **(23)**, we can derive the finite SNR diversity gain of node B as

$$d_{BR}(\rho,r) = -\frac{\rho}{P_{out}^{BR}(\rho,r)}\frac{\partial P_{out}^{BR}(\rho,r)}{\partial\rho}. \tag{39}$$

Theorem 6. *The analytical expression of the finite SNR diversity gain of node B for ABCom can be computed as*

$$d_{BR}(\rho,r) = -\frac{\rho}{P_{out}^{BR}(\rho,r)}(F_1+F_2), \tag{40}$$

where

- *When* $\Delta_R = \frac{\theta}{C_3}$, *the expressions of* F_1 *and* F_2 *can be rewritten as*

$$F_1 = \frac{m_B^{m_B}\theta^{m_B-1}e^{-\frac{\theta m_B}{\Omega_B\rho C_3}}(C_2\rho b-\theta C_3)}{\Gamma(m_B)\Omega_B^{m_B}\rho^{m_B+1}C_3^{m_B+1}}, \tag{41}$$

$$F_2 = \frac{(C_2\rho b-\theta C_3)G_3}{\Gamma(m_R)\Gamma(m_{RB})C_3^2}, \tag{42}$$

where $G_1 = \frac{m_R^{m_R}\theta^{m_R-1}e^{-\frac{\theta m_R}{\Omega_R C_3\rho}}}{\Omega_R^{m_R}C_3^{m_R-1}\rho^{m_R+1}}$, $G_2 = \frac{m_{RB}^{m_{RB}}\Delta_R^{m_{RB}-1}}{\Omega_{RB}^{m_{RB}}\rho^{m_{RB}+1}}e^{-\frac{\Delta_R m_{RB}}{\Omega_{RB}\rho}}$, *and* $G_3 = \Gamma\left(m_{RB},\frac{\theta m_{RB}}{C_3\Omega_{RB}\rho}\right)G_1 + \Gamma\left(m_R,\frac{\theta m_R}{C_3\Omega_R\rho}\right)G_2$.

- *When* $\Delta_R = \frac{\theta}{C_1}$, F_1 *and* F_2 *can be easily obtained as*

$$F_1 = \frac{m_B^{m_B}\theta^{m_B-1}e^{-\frac{\theta m_B}{\Omega_B C_1\rho}}[C_2\rho(1-b)-\theta C_1]}{\Gamma(m_B)\Omega_B^{m_B}\rho^{m_B+1}{C_1}^{m_B+1}}, \tag{43}$$

$$F_2 = \frac{[C_2\rho(1-b)-\theta C_1]G_4}{\Gamma(m_R)\Gamma(m_{RB})C_1^2}, \tag{44}$$

where $G_4 = \left(\Gamma\left(m_{RB},\frac{\theta m_{RB}}{C_1\Omega_{RB}\rho}\right)G_1 + \Gamma\left(m_R,\frac{\theta m_R}{C_1\Omega_R\rho}\right)G_2\right)$.

Proof: The proof of **Theorem 6** can be completed by simply taking the derivative of (20) with respect to ρ. ■

Remark 4. *From **Theorem 6**, we can find that with the increase of SNR, the finite SNR diversity gain decreases, which is roughly consistent with the varying trend of the OP slope. In addition, from the perspective of f-DMT, a smaller multiplexing gain results in a higher finite SNR diversity gain.*

IV. Numerical Results

In this section, the numerical results are obtained through 10^6 repeated trials of Monte Carlo simulations to confirm the correctness of the theoretical analysis in Section III. Unless otherwise specified, all parameter settings used in this section are given in Table I.

Fig. 2 plots the relationship between OPs and P_A under the condition of the nonideal and ideal conditions. First, we observe that the simulation results generated by the Monte Carlo method for ABCom and RCom are in good agreement with their analytical results. As shown in the Fig. 2, the ABCom curve represents the in-depth research work compared with [47], while the RCom curve can be represented as the simplified result[1] of [48]. Obviously, we can see that our work reduces the power consumption of the system within a certain range while achieving highly reliable long-distance transmission. As P_A increases, OPs decrease, which means that the reliability performance can be improved by increasing P_A. It is worth noting that for ABCom, the OPs approach to constants, indicating a zero-diversity order. The reason is that when P_A approaches infinity, SINR approaches a constant, which in turn leads the OP to approach a constant, indicating that there is an error floor for the system. In addition, we can also see that for either RCom or ABCom, the value of OP with ideal condition is always smaller than that of nonideal condition. This shows that nonideal condition has detrimental effects on the reliability of NOMA-assisted ABCom systems. From Fig. 2, it is also clear that the nonideal condition severity parameter has a greater effect on BD than node B for ABCom because BD applies SIC twice to decode signal $c(t)$. Similarly, we can clearly observe that the OP of RCom is significantly smaller than that of ABCom, which is also because for ABCom, BD has its own signal $c(t)$ to be decoded in the process of information transmission.

Fig. 3 depicts the OP of ABCom versus β adopting different power distribution coefficients with $\Omega_B = 2$, $\Omega_{DB} = 2$, $m_B = 1$ and $P_A = 0$ dBW. By comparison, it can be found that the OP of node B and the BD in the lower β region have different trends for the curve of β. Specifically, for node B, its OP increases with the increase of β; but for node BD, it shows that the OP first decreases and then increases with the increase of β. This means that with the increase of β, the interference of the reflection link will increase correspondingly, and it will be more difficult for node B to decode its own signal, leading to the deterioration of its reliable performance. The same is true for node BD. Similarly, when β is very large, the reliability performance of node BD deteriorates as the interference of

[1]Compared with [47], our study considered the more practical situation of existing ipSIC and ipCSI in ABCom system, which increased the practicability of the study. However, compared with the work in [48], we also consider the basic communication scenario of RCom system to serve as the benchmark for this considered system.

Table I
TABLE OF PARAMETERS FOR NUMERICAL SIMULATIONS.

Channel fading parameters	$m_B = 1$, $m_{AD} = 4$, $m_{DB} = 1$
Gamma distribution parameters of channel gains	$\Omega_B = 8$, $\Omega_{AD} = 2$, $\Omega_{DB} = 0.6$
Power distribution coefficients of NOMA	$b = 0.3$
Target data rate	$R = 0.05$
Average noise power	$\sigma^2 = 1$
Reflection parameter	$\beta = 0.4$
Severity parameter of ipSIC	$\xi = 0.3$
Error parameter of CSI	$\delta_e^2 = 0.04$
Accuracy-complexity trade-off parameters	$N = 20$, $K = 20$

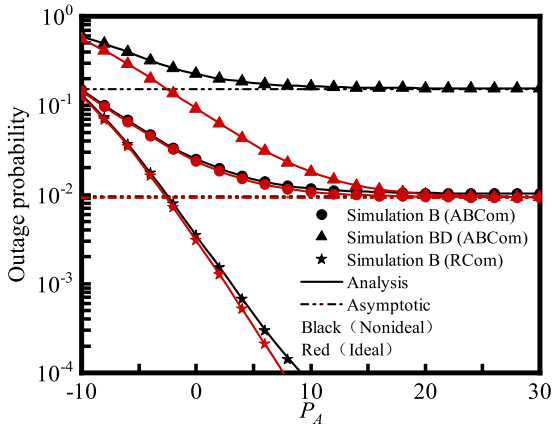

Fig. 2. The OP versus P_A with ideal and nonideal conditions.

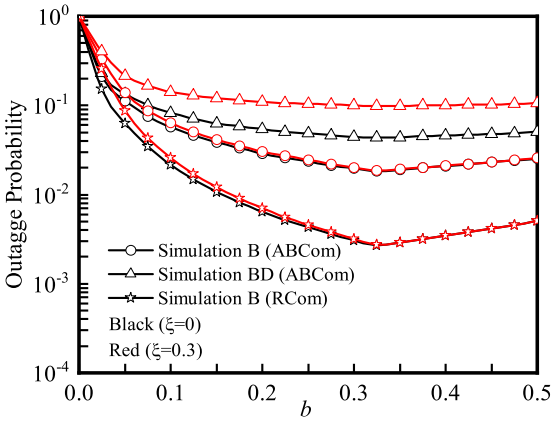

Fig. 4. The OP versus b with ideal and ipSIC conditions.

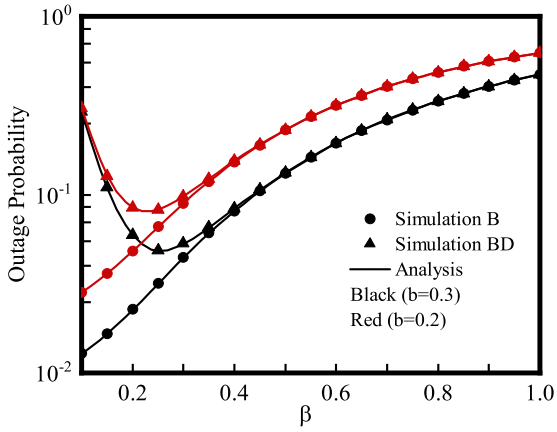

Fig. 3. The OP versus β with different power distribution coefficients.

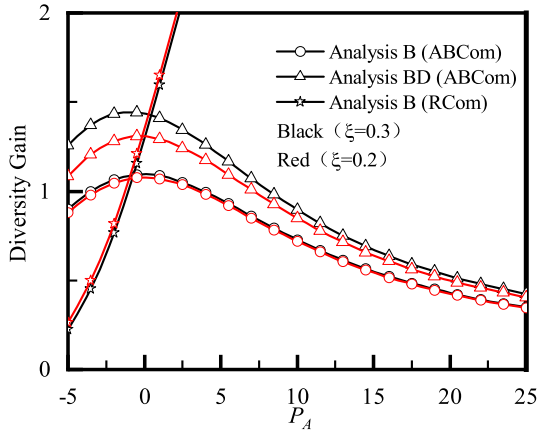

Fig. 5. Finite SNR diversity gain versus P_A with the different ipSIC parameters.

node B decoding its own signal becomes larger. However, when β is small, it becomes easy to decode the signal of node B, while it becomes difficult to decode that of node BD. Consequently, we can find from the Fig. 3 that when $\beta = 0.35$, the optimal reliability performance of node BD can be obtained. Longitudinally, when the power distribution coefficient b is reduced, the reliable performance of both nodes B and BD becomes worse.

Fig. 4 manifests the effect of power allocation factor b on the outage performance of the considered TW system under ideal and ipSIC conditions, where $R = 0.01$ and $P_A = 0$ dBW. As can be seen from Fig. 4, with the increase of b, the OP decreases first and then increases. This trend points out that there exists an optimal power allocation factor minimizing the OP, so that the system can obtain the best reliability. Specifically, we can find that the optimum reliability of the hybrid TW system is achieved when $b = 0.325$. On the other hand, the presence of ipSIC significantly reduces the reliability of the system, which verifies the correctness of **Remark 1**.

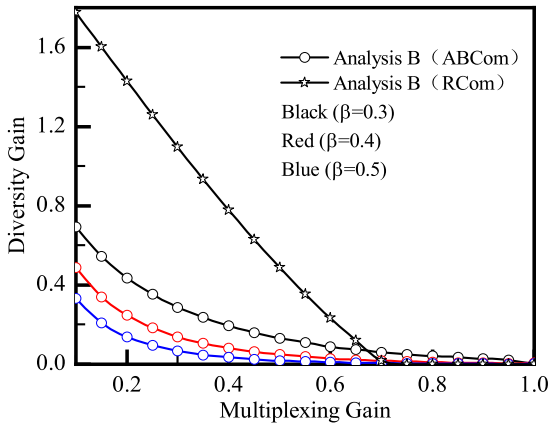

(a) f-DMT curves of B with different β.

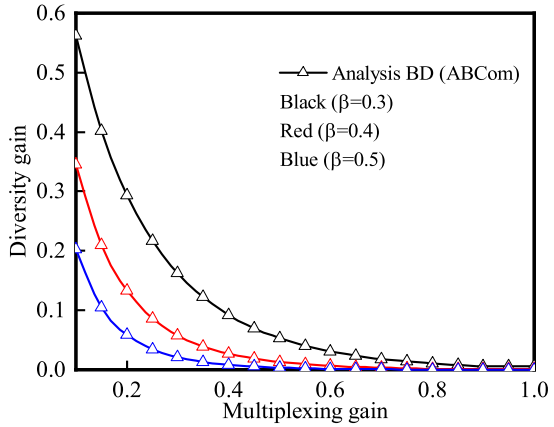

(b) f-DMT curves of BD with different β.

Fig. 6. f-DMT curves of B and BD with different β.

Fig. 5 demonstrates the finite SNR diversity gain versus P_A with different ξ. We understand that $d(\rho, r)$ is proportional to the negative slope of the OP curve. It can be seen from Fig. 2 that within the finite range of SNR for ABCom, the OPs decrease prominently, thus leading to appear a highlighted peak in a finite SNR diversity gain in Fig. 5. The RCom curve in the Fig. 5 can be viewed as a special case of [48], and our simulation results are similar to them[2]. Specifically, when $P_A = 0$ dBW, the maximum value of the finite SNR diversity gain can be acquired for node B. By the same token, for the BD, the peak value of finite SNR diversity gain can be obtained when $P_A = -1$ dBW. Similarly, for RCom, we can also clearly observe from Fig. 2 that OP decreases rapidly with the increase of P_A, resulting in the rapid increase of the finite SNR diversity gain for RCom as illustrated in Fig. 5. In addition, we can observe that for ABCom, the decrease of ξ leads to the deterioration of the finite SNR diversity gain so that the system can obtain poor reliability performance. Moreover, it is also apparent that ipSIC exists a greater impact on the BD, because the BD applies SIC more times than node B when decoding information. But for RCom, the decrease of ξ leads to the increase of the finite SNR diversity gain so as to result in better system reliability performance.

Fig. 6 presents the f-DMT of node B and the BD versus different β with $m_{DB} = 8$, $\Omega_{DB} = 6$, $\xi = 0.05$ and $P_A = 2$ dBW. As can be seen from the simulation results in Fig. 6, the finite SNR diversity gains of ABCom and RCom reduce with the increase of multiplexing gain. The results reveal that the diversity gains of both node B and node BD deteriorates, in which case the reliability performance of the system deteriorates. From the longitudinal observation of Fig. 6(a) and 6(b), it can be seen that the reduction of β can improve the finite SNR diversity gain, thereby improving the reliability performance.

V. Conclusion

In this paper, we studied the reliability performance of hybrid ABCom/RCom NOMA-assisted TW systems in the presence of ipSIC. The expressions of the OP of source and the BD and the finite SNR diversity gains of both were derived, and the asymptotic expressions of OP at high SNR were also derived. The derived results showed that ipSIC can degrade the reliability performance of the considered system to a certain extent. Through simulations of the proposed system under various setups, we can also come to a conclusion that f-DMT is easier to manage with a lower multiplexing gain and a lower reflection parameter, by which the proposed system achieves better reliability performance.

[2]The author of [46] considered the existence of wireless energy collection in RCom systems, but our work considers a more practical situation with ipSIC.

References

[1] X. You, C.-X. Wang, J. Huang *et al.*, "Towards 6G wireless communication networks: Vision, enabling technologies, and new paradigm shifts," *SCIENCE CHINA Information Sciences*, vol. 64, no. 1, pp. 1–74, 2021.

[2] Z. Zhang, Y. Xiao, Z. Ma *et al.*, "6G wireless networks: Vision, requirements, architecture, and key technologies," *IEEE Vehicular Technology Magazine*, vol. 14, no. 3, pp. 28–41, Jul. 2019.

[3] G. Wang, F. Gao, R. Fan *et al.*, "Ambient backscatter communication systems: Detection and performance analysis," *IEEE Transactions on Communications*, vol. 64, no. 11, pp. 4836–4846, Aug. 2016.

[4] X. Li, J. Zhang, C. Han, W. Hao, M. Zeng, Z. Zhu, and H. Wang, "Reliability and security of CR-STAR-RIS-NOMA assisted IoT networks," *IEEE Internet of Things Journal*, 2023.

[5] J.-H. Lee, S. S. Nam, and Y.-C. Ko, "Outage performance analysis of two-way full-duplex DF relaying networks with beamforming," *IEEE Transactions on Vehicular Technology*, vol. 69, no. 8, pp. 8753–8763, Aug. 2020.

[6] R. Duan, X. Wang, H. Yigitler *et al.*, "Ambient backscatter communications for future ultra-low-power machine type communications: Challenges, solutions, opportunities, and future research trends," *IEEE Communications Magazine*, vol. 58, no. 2, pp. 42–47, Feb. 2020.

[7] C. Chen, G. Wang, P. D. Diamantoulakis *et al.*, "Signal detection and optimal antenna selection for ambient backscatter communications with multi-antenna tags," *IEEE Transactions on Communications*, vol. 68, no. 1, pp. 466–479, Jan. 2020.

[8] S. Xiao, H. Guo, and Y.-C. Liang, "Resource allocation for full-duplex-enabled cognitive backscatter networks," *IEEE Transactions on Wireless Communications*, vol. 18, no. 6, pp. 3222–3235, Jun. 2019.

[9] Y. Zhang, F. Gao, L. Fan *et al.*, "Secure communications for multi-tag backscatter systems," *IEEE Wireless Communications Letters*, vol. 8, no. 4, pp. 1146–1149, Aug. 2019.

[10] V. Liu, A. Parks, V. Tallaand *et al.*, "Ambient backscatter: wireless communication out of thin air," *ACM SIGCOMM Computer Communication Review*, vol. 43, no. 4, pp. 39–50, 2013.

[11] W. Zhang, Y. Qin, W. Zhao *et al.*, "A green paradigm for Internet of Things: Ambient backscatter communications," *China Communications*, vol. 16, no. 7, pp. 109–119, Jul. 2019.

[12] X. Li, Y. Zheng, W. U. Khan *et al.*, "Physical layer security of cognitive ambient backscatter communications for green Internet-of-Things," *IEEE Transactions on Green Communications and Networking*, vol. 5, no. 3, pp. 1066–1076, Sep. 2021.

[13] G. Yang, Q. Zhang, and Y.-C. Liang, "Cooperative ambient backscatter communications for green Internet-of-Things," *IEEE Internet of Things Journal*, vol. 5, no. 2, pp. 1116–1130, Apr. 2018.

[14] Y. Ye, L. Shi, X. Chu *et al.*, "On the outage performance of ambient backscatter communications," *IEEE Internet of Things Journal*, vol. 7, no. 8, pp. 7265–7278, Aug. 2020.

[15] X. Li, Y. Zheng, M. D. Alshehri *et al.*, "Cognitive AmBC-NOMA IoV-MTS networks with IQI: Reliability and security analysis," *IEEE Transactions on Intelligent Transportation Systems*, pp. 1–12, Sep. 2021.

[16] A. Saffari, M. Hessar, S. Naderiparizi, and J. R. Smith, "Battery-free wireless video streaming camera system," in *2019 IEEE International Conference on RFID (RFID)*, 2019, pp. 1–8.

[17] V. Hansini, N. E. Elizabeth, R. Hemapriya, and S. Kavitha, "Secured backscatter communication between smart cars in a vehicular ad-hoc network," in *2016 10th International Conference on Intelligent Systems and Control (ISCO)*, 2016, pp. 1–4.

[18] L. Dai, B. Wang, Y. Yuan *et al.*, "Non-orthogonal multiple access for 5G: Solutions, challenges, opportunities, and future research trends," *IEEE Communications Magazine*, vol. 53, no. 9, pp. 74–81, Sep. 2015.

[19] S. Mounchili and S. Hamouda, "Pairing distance resolution and power control for massive connectivity improvement in NOMA systems," *IEEE Transactions on Vehicular Technology*, vol. 69, no. 4, pp. 4093–4103, Apr. 2020.

[20] Z. Ding, Y. Liu, J. Choi *et al.*, "Application of non-orthogonal multiple access in LTE and 5G networks," *IEEE Communications Magazine*, vol. 55, no. 2, pp. 185–191, Feb. 2017.

[21] S. Timotheou and I. Krikidis, "Fairness for non-orthogonal multiple access in 5G systems," *IEEE Signal Processing Letters*, vol. 22, no. 10, pp. 1647–1651, Oct. 2015.

[22] Q. Zhang, L. Zhang, Y.-C. Liang *et al.*, "Backscatter-NOMA: A symbiotic system of cellular and Internet-of-Things networks," *IEEE Access*, vol. 7, pp. 20 000–20 013, Feb. 2019.

[23] X. Li, H. Liu, G. Li *et al.*, "Effective capacity analysis of AmBC-NOMA communication systems," *IEEE Transactions on Vehicular Technology*, vol. 71, no. 10, pp. 11 257–11 261, Oct. 2022.

[24] X. Li, M. Zhao, M. Zeng *et al.*, "Hardware impaired ambient backscatter NOMA systems: Reliability and security," *IEEE Transactions on Communications*, vol. 69, no. 4, pp. 2723–2736, Apr. 2021.

[25] Y. Hong, W. Huang, and F. o. Chiu, "Cooperative communications in resource-constrained wireless networks," *IEEE Signal Processing Magazine*, vol. 24, no. 3, pp. 47–57, May 2007.

[26] L. Zhang, J. Liu, M. Xiao *et al.*, "Performance analysis and optimization in downlink NOMA systems with cooperative full-duplex relaying," *IEEE Journal on Selected Areas in Communications*, vol. 35, no. 10, pp. 2398–2412, Jul. 2017.

[27] J. Xue, M. Sellathurai, T. Ratnarajah *et al.*, "Performance analysis for multi-way relaying in rician fading channels," *IEEE Transactions on Communications*, vol. 63, no. 11, pp. 4050–4062, Nov. 2015.

[28] M. Z. Chowdhury, M. Shahjalal, S. Ahmed *et al.*, "6g wireless communication systems: Applications, requirements, technologies, challenges, and research directions," *IEEE Open Journal of the Communications Society*, vol. 1, pp. 957–975, Jul. 2020.

[29] A. Nosratinia, T. Hunter, and A. Hedayat, "Cooperative communication in wireless networks," *IEEE Communications Magazine*, vol. 42, no. 10, pp. 74–80, Oct. 2004.

[30] G. Kramer, M. Gastpar, and P. Gupta, "Cooperative strategies and capacity theorems for relay networks," *IEEE Transactions on Information Theory*, vol. 51, no. 9, pp. 3037–3063, Sep. 2005.

[31] Q. Zhang, J. Jia, and J. Zhang, "Cooperative relay to improve diversity in cognitive radio networks," *IEEE Communications Magazine*, vol. 47, no. 2, pp. 111–117, textbfFeb., 2009.

[32] L. Li, X. Zhou, H. Xu, G. Y. Li, D. Wang, and A. Soong, "Simplified relay selection and power allocation in cooperative cognitive radio systems," *IEEE Transactions on Wireless Communications*, vol. 10, no. 1, pp. 33–36, Jan. 2011.

[33] L. Zhang, J. Liu, M. Xiao, G. Wu, Y.-C. Liang, and S. Li, "Performance analysis and optimization in downlink noma systems with cooperative full-duplex relaying," *IEEE Journal on Selected Areas in Communications*, vol. 35, no. 10, pp. 2398–2412, Oct. 2017.

[34] Z. Yang, Z. Ding, P. Fan, and N. Al-Dhahir, "The impact of power allocation on cooperative non-orthogonal multiple access networks with SWIPT," *IEEE Transactions on Wireless Communications*, vol. 16, no. 7, pp. 4332–4343, Jul. 2017.

[35] C.-B. Le, D.-T. Do, A. Silva, W. U. Khan, W. Khalid, H. Yu, and N. D. Nguyen, "Joint design of improved spectrum and energy efficiency with backscatter NOMA for IoT," *IEEE Access*, vol. 10, pp. 7504–7519, 2022.

[36] J. Xue, S. Biswas, A. C. Cirik *et al.*, "Transceiver design of optimum wirelessly powered full-duplex MIMO IoT devices," *IEEE Transactions on Communications*, vol. 66, no. 5, pp. 1955–1969, May 2018.

[37] L. Zheng and D. Tse, "Diversity and multiplexing: a fundamental tradeoff in multiple-antenna channels," *IEEE Transactions on Information Theory*, vol. 49, no. 5, pp. 1073–1096, May 2003.

[38] R. Narasimhan, "Finite-SNR diversity-multiplexing tradeoff for correlated Rayleigh and Rician MIMO channels," *IEEE Transactions on Information Theory*, vol. 52, no. 9, pp. 3965–3979, Sep. 2006.

[39] Z. Yi, M. Ju, and I.-M. Kim, "Outage probability and optimum power allocation for analog network coding," *IEEE Transactions on Wireless Communications*, vol. 10, no. 2, pp. 407–412, Feb. 2011.

[40] T. Z. H. Ernest, A. S. Madhukumar, R. P. Sirigina *et al.*, "Outage analysis and finite SNR diversity-multiplexing tradeoff of hybrid-duplex systems for aeronautical communications," *IEEE Transactions on Wireless Communications*, vol. 18, no. 4, pp. 2299–2313, Apr. 2019.

[41] F. Parvaresh and H. Soltanizadeh, "Diversity-multiplexing trade-off of half-duplex single relay networks," *IEEE Transactions on Information Theory*, vol. 63, no. 3, pp. 1703–1720, Mar. 2017.

[42] X. Zhang, X. Yu, and S. Song, "Outage probability and Finite-SNR DMT analysis for IRS-aided MIMO systems: How large IRSs need to be?" *IEEE Journal of Selected Topics in Signal Processing*, vol. 16, no. 5, pp. 1070–1085, Aug. 2022.

[43] Y. Liu, Y. Ye, G. Yan *et al.*, "Outage performance analysis for an opportunistic source selection based two-way cooperative ambient backscatter communication system," *IEEE Communications Letters*, vol. 25, no. 2, pp. 437–441, Feb. 2021.

[44] X. Li, M. Zhao, Y. Liu *et al.*, "Secrecy analysis of ambient backscatter NOMA systems under I/Q imbalance," *IEEE Transactions on Vehicular Technology*, vol. 69, no. 10, pp. 12 286–12 290, Oct. 2020.

[45] J. Liu, J. Yu, R. Zhang, S. Wang, K. Yang, and J. An, "Covert MIMO ambient backscatter communication," *IEEE Transactions on Communications*, 2023.

[46] W. Zhao, G. Wang, S. Atapattu, R. He, and Y.-C. Liang, "Channel estimation for ambient backscatter communication systems with massive-antenna reader," *IEEE Transactions on Vehicular Technology*, vol. 68, no. 8, pp. 8254–8258, Aug. 2019.

[47] H. Wang, J. Jiang, G. Huang *et al.*, "Physical layer security of two-way ambient backscatter communication systems," *Wireless Communications and Mobile Computing*, 2022.

[48] Y. S. Rao, A. S. Madhukumar, and S. R. Prasad, "Wireless energy harvesting-based relaying: A Finite-SNR diversity-multiplexing tradeoff perspective," *IEEE Transactions on Green Communications and Networking*, vol. 4, no. 1, pp. 277–288, Mar. 2020.